International Journal of Adhesion & Adhesives 56 (2015) 53–60

Contents lists available at ScienceDirect

International Journal of Adhesion & Adhesives

journal homepage: www.elsevier.com/locate/ijadhadh

Predicting impact shear strength of phenolic resin adhesive blended with nitrile rubber

Tadaharu Adachi [a,*], Takao Kataoka [b], Masahiro Higuchi [c]

[a] Department of Mechanical Engineering, Toyohashi University of Technology, Toyohashi, Japan
[b] Department of Mechanical Sciences and Engineering, Tokyo Institute of Technology (Present JR Central Railway Co., Ltd.), Tokyo, Japan
[c] Faculty of Mechanical Engineering, Kanazawa University, Kanazawa, Japan

ARTICLE INFO

Article history:
Accepted 3 June 2014
Available online 23 July 2014

Keywords:
Impact
Phenolic
Strain rate-temperature dependence
Shear strength

ABSTRACT

The impact shear strength of phenolic resin adhesive blended with nitrile rubber in a double-lap steel joint was measured to discuss the applicability of the strain rate-temperature equivalent principle. This strain rate-temperature equivalent principle was confirmed to be applicable to the quasi-static shear strengths of the adhesive. Because phenolic resin adhesive blended with nitrile rubber was in the glass transition state under a quasi-static deformation at room temperature and its adhesive strength was sensitive to the strain rate, the impact strength of the adhesive could not be predicted without the strain rate-temperature equivalent principle. Instead, the impact strength of the adhesive measured by using a manufactured impact testing machine could be predicted approximately with quasi-static results at low temperature by using the principle. The strain rate-temperature equivalent principle was clarified to be sufficient for predicting impact strengths without the need for impact testing.

1. Introduction

Adhesive bonding is applied to joint structural components in several mechanical structures. The strengths of adhesive joints are important to ensure the reliability of structures [1]. Because, in many cases, this bonding is subjected to impact loads, the impact strength of the adhesive also needs to be evaluated. Several researchers clarified the impact strengths of adhesive joints by using a split Hopkinson pressure bar testing [2–9]. Some researchers have clarified the strengths by using drop weight testing and pendulum testing [10–15].

The dependences of high strain rates on adhesions were discussed in almost all pieces of research related to impact strengths. Temperature dependence needs to be considered because of thermo-viscoelasticity in polymer bonds as well as strain rate dependence on the impact strengths of adhesive joints, [16,17]. The dependences of strain rates and temperatures on deformation are known as the temperature-time equivalent principle in thermo-viscoelastic theory [18,19]. The strengths and fracture toughnesses of many polymers were clarified to be governed by this principle in several pieces of research [19–30]. Some studies have shown that the principle can be applied to adhesive joints or bonds. Gent and Petrich [31] clarified that the peel energy of styrene-butadiene rubber adhesives on a polyester film followed the time-temperature equivalent principle above the glass transition temperature with the Williams–Landel–Ferry (WLF) equation [18,19]. Gent and Kinloch [32] expressed adhesive fracture energy as a function of temperature and deformation rate of copolymer of butadiene and styrene/mylar-coated steel joints on the basis of the strain rate-temperature equivalent principle with the WLF equation. Aubrey and Sherriff [33] investigated the peel adhesions of mixtures with various proportions of natural rubber and each of two tackifier resins, a poly-β-pinene and a modified pentaerythritol rosin ester, in joining a flexible polyester strip to a plane glass substrate and confirmed that the time-temperature equivalent principle could be applied to the adhesion. Lim and Mizumachi [34,35] investigated the critical mode I and II strain energy release rates of polyurethane adhesives between Japanese birch plates. They reported that master curves based on the rate-temperature equivalent principle could be applied to the critical strain energy release rates. Derail et al. [36,37] reported the peeling properties of polybutadiene/tackifying resin compatible blends and found the master curve of the peeling force. Guiu and Shanahan [38] used a peel test to investigate adhesion between high-density polyethylene (HDPE) with an inner layer of an ethylene/vinyl alcohol copolymer (EVOH) in a five-layer structural system that consisted of two outer strata of HDPE with an inner layer of EVOH. They found that the strain rate- and temperature-dependences of peel energy can be described by using a

* Correspondence to: Department of Mechanical Engineering, Toyohashi University of Technology, 1-1 Hibarigaoka, Tempaku, Toyohashi 441-8580, Japan. Tel.: +81 532 44 6664; fax: +81 532 44 6661.
E-mail address: adachi@me.tut.ac.jp (T. Adachi).

http://dx.doi.org/10.1016/j.ijadhadh.2014.07.010
0143-7496/

time–temperature superposition with an Arrhenius-based relation [18,19]. As described above, the report on the time-temperature equivalent principle was limited to the static and quasi-static strengths of the adhesives. However, the impact strengths of adhesive joints determined on the basis of time-temperature superposition have not been discussed. The applicability of the time-temperature equivalent principle to impact strengths needs to be considered to predict impact strengths from static ones under a different temperature environment because a specific apparatus is required to measure the impact adhesive strength and managing the deformation rate is not easy in impact testing.

We describe how the impact shear strength of phenolic resin adhesive blended with nitrile rubber in a double-lap joint was measured to discuss the applicability of the strain rate-temperature equivalent principle. Quasi-static tests were done at different strain rates under several temperatures to draw a master curve of the shear strength on the basis of the strain rate-temperature equivalent principle. Impact tests were conducted by using a manufactured pendulum testing machine to measure strengths under high strain rates. On the basis of a comparison of the impact shear strengths with the quasi-static strengths on the master curve, the prediction of the impact strength of the adhesive was discussed.

2. Specimen preparation

Simple double-lap joints with phenolic resin adhesive blended with nitrile rubber were prepared to measure the shear strength of the adhesive without deformation caused by a specimen bending. The joints consisted of three steel plate adherends having 10 mm in overlap length, and their geometric configuration is shown in Fig. 1. The specimens for impact tests had holes near both ends to fix them to the impact testing machine explained in Section 3, although specimens for quasi-static tests did not. The distance between the hole and the adhesive region was lengthened in order to average stress dispersed due to the holes on the basis of the dynamic stress concentration around a hole [39]. The Young's modulus, yield stress, and ultimate tensile strength of the steel were 211 GPa, 261 MPa, and 349 MPa, respectively. Surfaces of the steel adherends were treated by shot-peening to increase adhesive strength. The average surface roughness after the shot-peening was 7.4 μm. The adherends were bonded with resin adhesive under a pressure of 2.5 MPa and at a temperature of 503 K for 30 min. Several prepared specimens were cut after bonding to measure the thickness of the adhesive layer between the steel plates with a scanning electron microscope (JSM-T200, Jeol). The average thickness of the adhesive layers was 30 μm.

3. Experimental procedure

3.1. Quasi-static test

Quasi-static tests were conducted by using a tensile testing machine (8501, Instron) with tensile displacement rates of 0.01, 1, and 100 mm/min for each temperature of 203, 223, 253, 293, 343, and 423 K in a thermostatic oven (3119-007, Instron). The total test conditions were 18 combinations of 3 displacement rates with 6 temperatures. Ten specimens at the standard condition, a displacement rate of 1 mm/min and room temperature of 293 K, were measured, though one specimen for the other conditions was measured. The load was measured with a load cell in a testing machine, and deformation of the specimens was also measured in a gage length of 25 mm by using an extensometer (Fig. 2). The deformation included deformations of the adhesive and the adherends. Because the loading at the breaking of the resin adhesive was below the yielding of the steel adherends, the elastic deformations of the adherends were eliminated from the measured deformation in the gage length to evaluate the deformation of the adhesive layer. The average shear stress, which was the tensile force divided by the initial overlap area, was used to express the strength of the joints. The average shear strain rate was defined as the ratio of the deformation rate of the adhesive layer and the average thickness of the adhesive.

3.2. Impact test

(a) Impact testing machine

An impact testing machine was developed to measure impact shear strength, as shown in Fig. 3(a). The machine had a pendulum and an impactor. The impactor consisted of two steel bars that were 25 mm wide, 30 mm high, 300 mm long, approximately 0.7 kg in weight, and were rounded at the collision ends. The right side of each specimen was mounted at the left end of a dynamic load cell, shown in Fig. 3(a). The left end was connected by pins at Block D, which moved freely on a steel base. The right end of the dynamic load cell was fixed through Block E on the steel base. The impactor was collided to the Block D to apply impact tensile load to the specimen. Two strain gages (KFG-2-120-C1-11, Kyowa) were attached on both sides of Adherend A to confirm that the strain histories measured from the strain gages coincided by simultaneously colliding the two bars of the impactor to Block D (Fig. 1). The impact tests were conducted at room temperature, 293 K. Because the overlap length of the specimen was 10 mm, stress distribution in the adhesive region could be

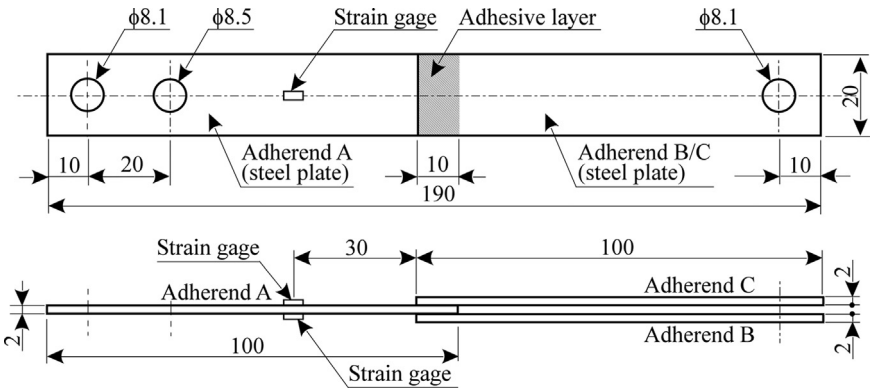

Fig. 1. Specimen. All dimensions are in mm. Specimens for impact tests had holes near both ends to fix them to impact testing machine, although specimens for quasi-static tests did not. Two strain gages on both sides of Adherend A were used in impact test to confirm simultaneous collision of two bars in impactors.

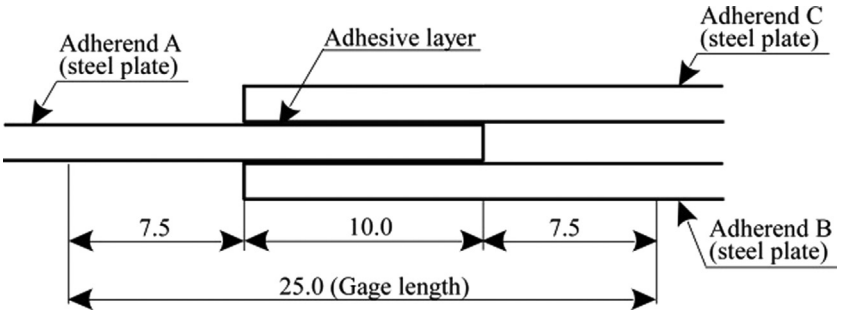

Fig. 2. Gage length in quasi-static test. All dimensions are in mm.

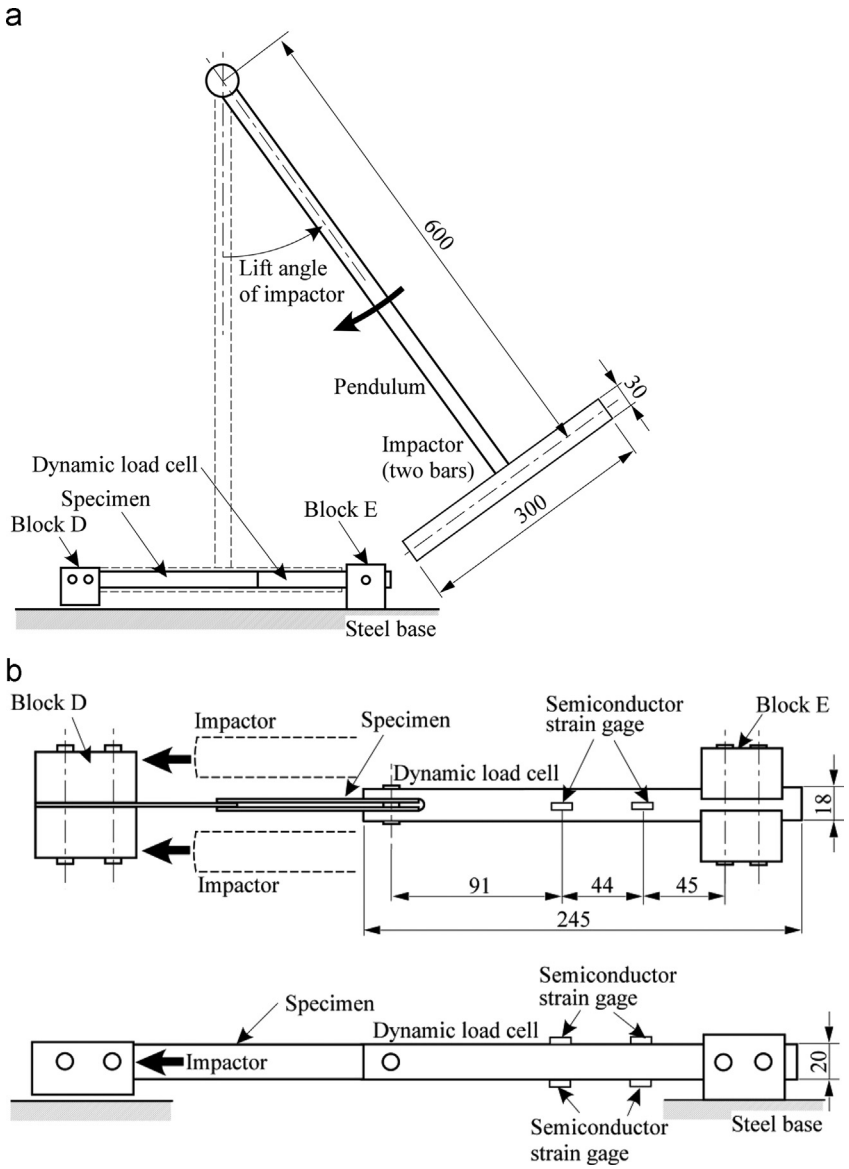

Fig. 3. Impact testing machine. (a) Overall view. (b) Dynamic load cell. All dimensions are in mm. Two strain gages on both sides of Adherend A (Fig. 1) are omitted in Fig. 3(b).

approximated to be uniform in the loading. Therefore, shear stress was evaluated by using the impact tests.

(b) Measurement system

The dynamic load cell was manufactured to measure a load widely ranging from impulsive to quasi-static. As shown in Fig. 3(b), the dynamic load cell for measuring the impact load applied to the specimen was a steel bar (Young's modulus: 209 GPa, density: 7850 kg/m^3) that was 18 mm wide, 20 mm high, and 245 mm long. Two semiconductor strain gages (KSP-2-120, Kyowa) were attached on both lateral sides of the dynamic load cell at two positions to measure longitudinal strains. Data of the strain gages were stored through dynamic strain meters (6M91, NEC Sanei) to a data logger (8835, Hioki). Every result was measured at an interval of 1 μs.

The impact load was calculated from two strain histories and by using the following method. Fig. 4 denotes an analytical model of the dynamic load cell. The impact load was applied to the left end of the dynamic load cell. Strain histories at two positions, ε_A and ε_B, were measured with the strain gages. The mechanical behavior of the dynamic load cell is governed by an equation for one-dimensional wave motion.

$$\frac{\partial^2 u(x,t)}{\partial x^2} = \frac{\rho}{E}\frac{\partial^2 u(x,t)}{\partial t^2}, \tag{1}$$

where u, E, and ρ denote axial displacement, longitudinal elastic modulus, and density of the dynamic load cell. Here, x and t are a coordinate defined in Fig. 4 and time. After applying the Laplace transformation to Eq. (1), the general solution is derived as

$$\overline{u} = A_1 \exp\left(\frac{s}{C}x\right) + A_2 \exp\left(-\frac{s}{C}x\right), \tag{2}$$

where A_i is an unknown coefficient determined by the boundary conditions and C is the velocity of a longitudinal wave defined as

$$C = \sqrt{\frac{E}{\rho}}.$$

The Laplace transformation is defined by

$$\overline{u}(s) = \int_0^\infty u(t) \exp(-st)\, dt.$$

The measured strain histories are given as the boundary conditions:

$$\frac{\partial u}{\partial x} = \varepsilon_A(t) \text{ at } x = \frac{L}{2},$$
$$\frac{\partial u}{\partial x} = \varepsilon_B(t) \text{ at } x = \frac{3L}{4}, \tag{3}$$

where L is length of the dynamic load cell defined in Fig. 4. By substituting Eq. (2) into Eq. (3), the unknown coefficients are determined as

$$A_1 = \frac{C}{2s}\frac{1}{\sin h\left(\frac{Ls}{4C}\right)}\left\{-\overline{\varepsilon}_A(s)\exp\left(-\frac{3Ls}{4}\right) + \overline{\varepsilon}_B(s)\exp\left(-\frac{Ls}{2}\right)\right\}$$
$$A_2 = \frac{C}{2s}\frac{1}{\sin h\left(\frac{Ls}{4C}\right)}\left\{-\overline{\varepsilon}_A(s)\exp\left(\frac{3Ls}{4}\right) + \overline{\varepsilon}_B(s)\exp\left(\frac{Ls}{2}\right)\right\} \tag{4}$$

The impact load is given as follows.

$$\overline{F}(s) = AE\frac{d\overline{u}}{dx} \quad \text{at} \quad x = 0, \tag{5}$$

where A is the cross-sectional area of the dynamic load cell. By using an inverse Laplace transformation of Eq. (5) with Eq. (4), the solution is derived.

$$F(t) = AE\left\{\varepsilon_A\left(t - \frac{L}{2C}\right) + \varepsilon_B\left(t + \frac{L}{2C}\right) + \varepsilon_A(t) - \varepsilon_B\left(t - \frac{L}{4C}\right) - \varepsilon_B\left(t + \frac{L}{4C}\right)\right\} \tag{6}$$

By using Eq. (6) with measured strain histories, ε_A and ε_B, the impact load can be calculated.

Displacement at the left side of Block D measured by using an optical displacement transducer (100B, Zimmner, resolution: 1 μm, frequency response: until 300 kHz) was approximated as the deformation of the specimen.

The impact velocity of the impactor was controlled by using the initial lift angle of the pendulum. The results were evaluated in a manner similar to the one in the quasi-static test, namely, average shear stress and strain rate.

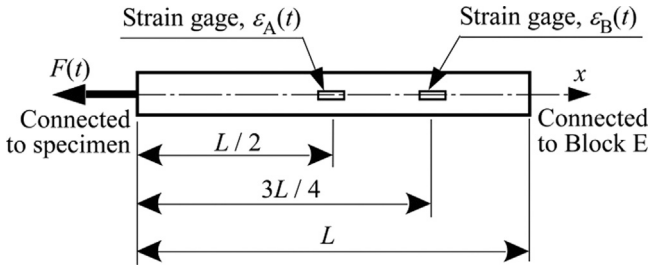

Fig. 4. Analytical model of dynamic load cell used to calculate impact load. Left end of dynamic load cell is connected to specimen. Right end is connected to Block E.

4. Experimental results

4.1. Quasi-static test

Several average shear stress–deformation curves of the specimens were measured under different temperatures and displacement rates. The stress–deformation curves are shown in Fig. 5 to express the dependences of the temperature and deformation rate on the curves. The stress–deformation curves were nonlinear except in the case of the lowest temperature, 203 K. The initial slopes of the stress–displacement curves reduced under low displacement rates or/and high temperatures because of thermo-viscoelastic properties. The ultimate shear stress, namely, apparent shear strengths, also decreased for low displacement rates and high temperatures. Therefore, the mechanical properties of the adhesive were found to be strongly dependent on the temperature and deformation rates.

After the quasi-static tests, we observed fracture surfaces on the adherends of the specimens by using an optical microscope (SHZ-ILLD, Olympus). Fracture for every specimen was found to occur only on interfaces between the adhesive and the adherend, namely, interfacial failures occurred because the adhesives

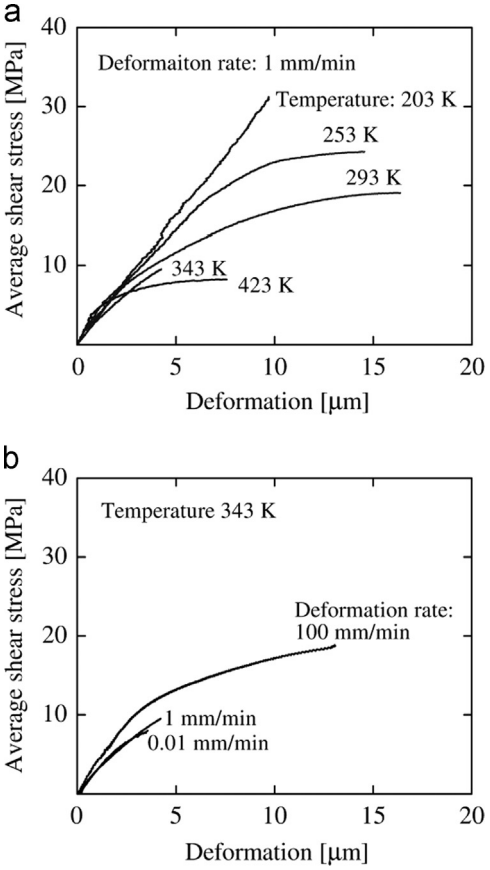

Fig. 5. Average shear stress–deformation curves in quasi-static tests. (a) Temperature dependence at deformation rate of 1 mm/min. (b) Deformation rate dependence at 343 K. These graphs were typical average shear stress–deformation curves.

remained on either the surface of Adherend A or those of Adherends B and C (Fig. 6). Digital images of the fracture surfaces taken with the optical microscope were binarized to clarify any remaining adhesives on the adherends in the images. Shown in Fig. 7(a) are binarized images of the surfaces of Adherends B and C for the 10 specimens tested at a deformation rate of 1 mm/min and temperature of 293 K. The black and white regions in the figure denote adhesives on the adherends and surfaces of the adherends, respectively. The adhesive only near the circumferential edge remained on Adherends B and C, although most of the

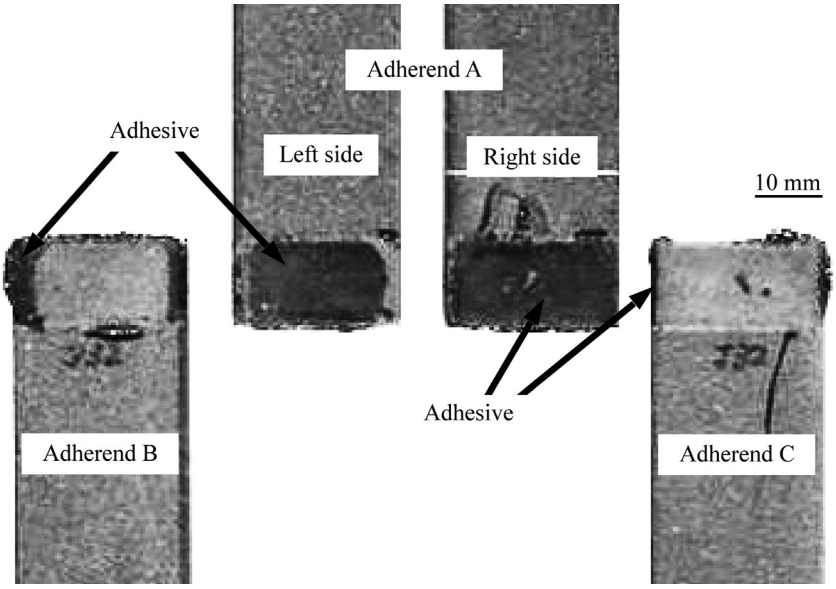

Fig. 6. Specimen after quasi-static tests. Temperature and deformation rate of quasi-static test were 293 K and 1 mm/min.

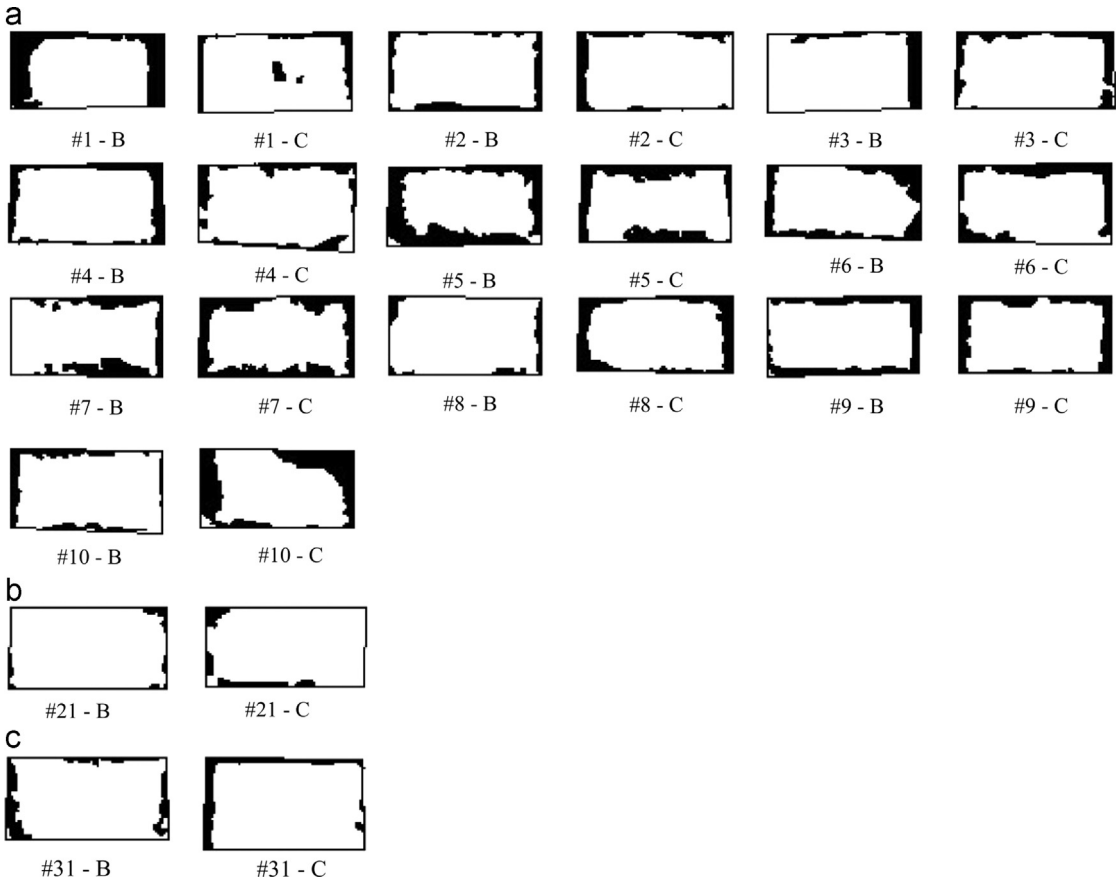

Fig. 7. Binarized fracture surfaces. (a) Fracture surface images of 10 specimens at 293 K and 1 mm/min. Fracture surfaces of #1-B and -C were binarized from images in Fig. 6. (b) Fracture surface image of specimen with maximum apparent shear strength: 31.2 MPa (test condition: 203 K and 1.0 mm/min). (c) Fracture surface image of specimen having minimum apparent shear strength: 5.4 MPa (test condition: 423 K and 0.01 mm/min). Black and white regions in Fig. 8 denote adhesives on adherends and their surfaces. Here "#1-B" and "#1-C" mean fracture surfaces on Adherends B and C of specimen #1.

adhesive remained on the surface of Adherend A. Fig. 7(b) and (c) show the binarized images of the fracture surfaces of the specimens with maximum and minimum values of the apparent shear strengths within all quasi-static tests. The characteristics of the images in Fig. 7 were not recognized only from observation of the fracture surfaces. The ratios of the remaining adhesive area to the initial area of the adhesive layer in the images of Fig. 7 were calculated to quantitatively consider the characteristics of the fracture surfaces related to the apparent shear strengths. The ratios are plotted in Fig. 8. The results under the deformation rate of 1 mm/min and temperature of 293 K were expressed by using average value with error bars denoting a two-sided 95% confidence interval. However, the ratios did not correlate to the apparent shear strength. Therefore, fractures for every test condition were clarified to occur with the same interfacial failure mode.

4.2. Impact test

Some histories of the shear stress and deformation of the specimens with lift angles of the pendulum, about 50 and 115 degrees, are plotted in Fig. 9. For the lift angle of 50 degrees (Fig. 9(a)), the average shear stress reached a maximum at 17 MPa at 0.13 ms. At this time, fracture of the adhesive layer occurred. After that the fracture was expanded and finally broke completely at 0.33 ms. The deformation rate was kept constant until the specimen broke. For the lift angle of 115 degrees (Fig. 9(b)), the average shear stress increased until 32 MPa at 0.08 ms and the adhesive layer was broken completely at 0.15 ms. The shear stress was fluctuated due to vibration of the load cell after the specimen broke. The average shear stress rate was dependent on the lift angle, namely, impact velocity of the impactor to Block D. In this case, the deformation was also linear to time. Therefore, by using the manufactured testing machine, impact tests could be conducted under a constant deformation rate controlled by the lift angle of the pendulum.

The impact apparent shear strengths of the adhesive when the lift angles of the pendulum were 50 and 115 degrees are summarized in Fig. 10. The apparent shear strengths increased when the impact velocity of the impactor were higher, although the measured results were scattered a little. The fracture surfaces on the adherends after the impact tests were observed after the tests. The failure modes of the fracture surfaces were confirmed to be the same as the ones in the quasi-static tests.

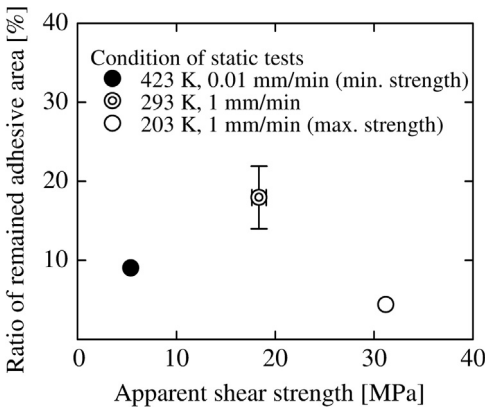

Fig. 8. Ratios of remaining adhesive area on fracture surface of Adherends B and C to overlap area. Double circle and their error bars denote mean values and 95% confidence intervals of ratios calculated from binarized images in Fig. 7(a). Values of open and solid circles were calculated from binarized images in Fig. 7(b) and (c), respectively.

5. Discussion

The relationship between the apparent shear strengths and strain rates in the quasi-static tests is illustrated in Fig. 11. The average shear strengths were not clearly dependent on the strain rate in Fig. 11 because the strengths had a different tendency for different temperatures.

To consider the strain rate dependence of the shear strengths, the strain rate-temperature equivalent principle was applied to the results in Fig. 11. By applying a similar way to the time-temperature equivalent principle of the thermo-viscoelastic property [17,18], the quasi-static shear strengths under different

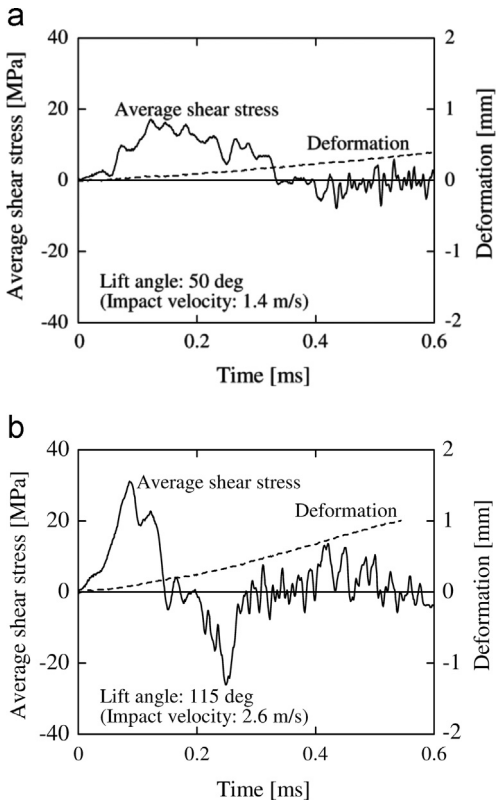

Fig. 9. Histories of average shear stress and deformation in impact tests. (a) Lift angle of pendulum, 50 deg. (b) Lift angle of pendulum, 115 deg. Solid and broken lines denote histories of average shear stress and deformation. Temperature was 293 K.

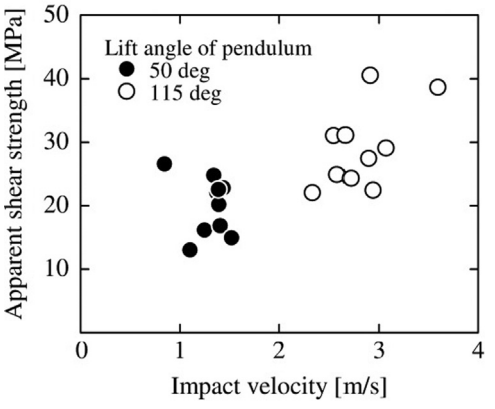

Fig. 10. Impact apparent shear strengths. Ten specimens were measured for each pendulum angle at 293 K.

temperatures and strain rates were shifted horizontally along the strain rate axis to describe the master curve of the apparent shear strength at standard temperature. The shifted strain rate and the shift value along the strain rate axis are called "reduced strain rate" and "shift factor", respectively. The shifted master curve of the shear strengths is plotted at a standard temperature of 293 K in Fig. 12. The shift factor of the master curve shown as an Arrhenius plot, is denoted in Fig. 13. The strain rate-temperature equivalent principle was confirmed to be applicable to the apparent shear strengths because the strengths were present roughly along one curve. The strengths increased rapidly within the strain rate ranges from 10^{-4} to 10^{-2} s^{-1}. This means that glass transition from a rubbery to a glassy state occurred at the strain rate region under a temperature of 293 K. The shift factor was confirmed to be governed by a thermally activated process because the shift factor could be expressed as bilinear in the Arrhenius plot.

The data of the impact apparent shear strengths in Fig. 10 were superimposed on the master curve of Fig. 12. The impact data were in rough alignment with the master curve. The validity of the strain rate-temperature equivalent principle was also confirmed even for the impact strengths. Because the phenolic resin adhesive blended with nitrile rubber was in the glass transition state under quasi-static deformation (strain rates from 10^{-4} to 1 s^{-1}) at 293 K and the shear strength varied significantly at strain rates from 10^{-4} to 1 s^{-1}, the impact strength of the adhesive could not be predicted without using the strain rate-temperature equivalent principle, namely the master curve (Fig. 12) with the shift factor (Fig. 13). In the same way, the impact strength of the adhesive could be approximately predicted on the basis of the results of the quasi-static test at low temperatures found by using the strain rate-temperature equivalent principle without the impact testing. The strain rate-temperature equivalent principle was found to be sufficient for predicting the impact strengths of phenolic resin adhesive blended with nitrile rubber.

6. Conclusion

We describe how the impact apparent shear strength of phenolic resin adhesive blended with nitrile rubber in a double-lap joint was measured to discuss the applicability of the strain rate-temperature equivalent principle. This principle was confirmed to be applicable to the quasi-static apparent shear strengths of the adhesive. Because phenolic resin adhesive blended with nitrile rubber was in the glass transition state under quasi-static deformation at room temperature and its adhesive strength was sensitive to the strain rate, the impact strength of the adhesive could not be predicted without using the strain rate-temperature equivalent principle. Instead, the impact strength of the adhesive measured by using the manufactured impact testing machine could be predicted approximately with the quasi-static results at low temperature by using the principle. Therefore, the principle was found

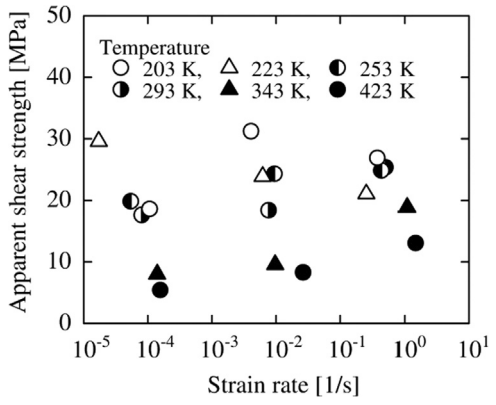

Fig. 11. Relationship between apparent shear strength and strain rate. Results were all data in quasi-static tests under different temperatures and strain rates.

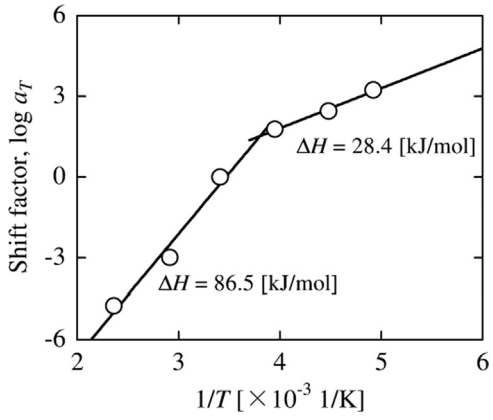

Fig. 13. Shift factor of apparent shear strength. Shift factor was used to draw master curve in Fig. 12. Here, ΔH denotes apparent activated energy.

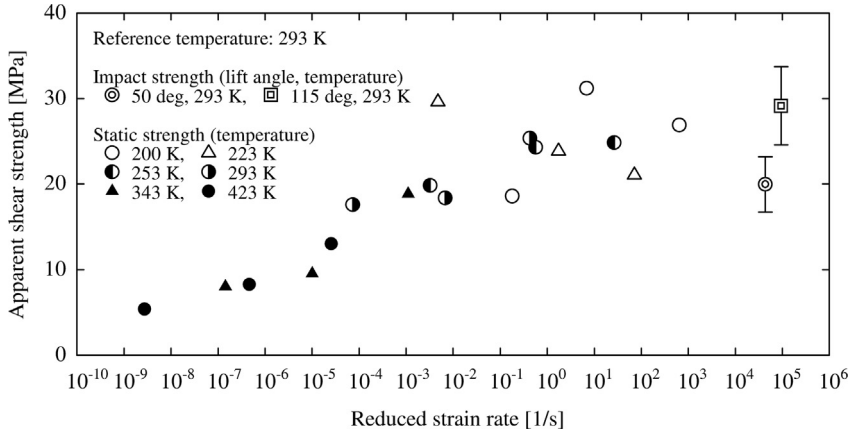

Fig. 12. Master curve of apparent shear strength. Master curve was drawn as strain dependence property of apparent shear strength at reference temperature, 293 K, by shifting results in Fig. 11 along strain rate axis with impact strengths.

to be sufficient for predicting the impact strengths without the need for impact testing.

References

[1] Baldan A. Adhesively-bonded joints in metallic alloys, polymers and composite materials: mechanical and environmental durability performance. J Mater Sci 2004;39:4729–97.
[2] Yokoyama T, Shimizu H. Determination of impact shear strength of adhesive bonds with the split Hopkinson bar. Trans Jpn Soc Mech Eng Part A 1997;63:2604–9.
[3] Sato C, Ikegami K. Strength of adhesively-bonded butt joints of tubes subjected to combined high-rate loads. J Adhes 1999;70:57–73.
[4] Yokoyama T. Experimental determination of impact tensile properties of adhesive butt joints with the split Hopkinson bar. J Strain Anal Eng Des 2003;38:233–45.
[5] Yokoyama T, Nakai K. Determination of impact tensile properties of structural epoxy adhesive butt joints using a hat-shaped specimen. (IV France). J Phys 2006;134:789–95.
[6] Srivastava V, Shukla A, Parameswaran V. Experimental evaluation of the dynamic shear strength of adhesive-bonded lap joints. J Test Eval 2000;28:438–42.
[7] Chen X, Li Y. An experimental technique on the dynamic strength of adhesively bonded single lap joints. J Adhes Sci Tech 2010;24:291–304.
[8] Challita G, Othman R. Finite-element analysis of SHPB tests on double-lap adhesive joints. Int J Adhes Adhes 2010;30:236–44.
[9] Challita C, Othman R, Casarai P, Khalil K. Experimental investigation of shear dynamic behavior of double-lap adhesively bonded joints on a wide range of strain rates. Int J Adhes Adhes 2011;31:146–53.
[10] Beevers A, Ellis MD. Impact behaviour of bonded mild steel lap joints. Int J Adhes Adhes 1984;4:13–6.
[11] Jordan M. The instrumented guillotine impact testing apparatus. Int J Adhes Adhes 1988;8:39–46.
[12] Bezemer AA, Guyt CB, Vlot A. New impact specimen for adhesives: optimization of high-speed-loaded adhesive joints. Int J Adhes Adhes 1988;18:255–60.
[13] Adams RD, Harris JA. A critical assessment of the block impact test for measuring the impact strength of adhesive bonds. Int J Adhes Adhes 1996;16:61–71.
[14] Goglio, Rossetto L. Impact rupture of structural adhesive joints under different stress combination. Int J Impact Eng 2008;35:635–43.
[15] Kihara K, Isono H, Yamabe H, Sugibayashi T. A study and evaluation of the shear strength of adhesive layers subjected to impact loads. Int J Adhes Adhes 2003;23:253–9.
[16] Adamvalli M, Parameswaran V. Dynamic strength of adhesive single lap joints at high temperature. Int J Adhes Adhes 2008;28:321–7.
[17] Banea MD, da Silva LFM, Campilho RDSG. Temperature dependence of the fracture toughness of adhesively bonded joints, J Adhes Sci Tech, 24 (2019) 2011-2026.
[18] Ferry JD. Viscoelastic properties of polymers. New York: John-Wiley & Sons; 1970; 292–351.
[19] Ward IM. Mechanical properties of solid polymers. Chichester: John-Wiley & Sons; 1985; 133–46.
[20] Buche F. Tensile strength of plastics above the glass temperature. J Appl Phys 1955;26:1133–40.
[21] Smith TL. Dependence of the ultimate properties of a GR–S rubber on strain rate and temperature. J Polym Sci 1958;32:99–112.
[22] Greensmith HW, Mullins L, Thomas AG. Rupture of rubber. Trans Soc Rheol 1960;4:179–89.
[23] G'sell C, Jonas JJ. Yield and transient effects during the plastic deformation of solid polymers. J Mater Sci 1981;16:1956–74.
[24] Kasamori M, Ootsuka T, Shimbo M, Miyano Y. Time-temperature dependencies of mechanical properties of high temperature epoxy resin and CFRP laminates using the resin. J Soc Mater Sci Jpn 1992;41:465–9.
[25] Miyano Y, McMurray MK, Kitade N, Nakada M, Mohri M. Loading rate and temperature dependence of flexural behavior of unidirectional pitch-based CFRP laminates. Composites 1995;26:713–7.
[26] Atkins AG, Lee CS, Caddell RM. Time-temperature dependent fracture toughness of PMMA. J Mater Sci 1975;10:1381–93.
[27] Wu J, Mai YW, Cotterrell B. Fracture toughness and fracture mechanisms of PBT/PC/IM blend. J Mater Sci 1994;28:3373–84.
[28] Araki W, Adachi T, Gamou M, Yamaij A. Time-temperature dependence of fracture toughness for bisphenol A epoxy resin. Proc Inst Mech Eng Part L J Mater Des Appl 2002;216:79–84.
[29] Adachi T, Osaki M, Yamaji A, Gamou M. Time-temperature dependence of the fracture toughness of a poly (phenylene sulphide) polymer. Proc Inst Mech Eng Part L J Mater Des Appl 2003;217:29–34.
[30] Araki W, Asahi D, Adachi T, Yamaji A. Time-temperature dependency of mode II fracture toughness for bisphenol A-type epoxy resin. J Appl Polym Sci 2005;96:51–5.
[31] Gent AN, Petrich RP. Adhesion of viscoelastic materials to rigid substrates. Proc R Soc London, Ser A 1969;310:433–48.
[32] Gent AN, Kinloch AJ. Adhesion of viscoelastic materials to rigid substrates. III. Energy criterion for failure. J Polym Sci, Part A: Polym Chem 1971;2 (9):659–68.
[33] Aubrey DW, Sherriff M. Peel adhesion and viscoelasticity of rubber–resin blends. J Polym Sci, Part A: Polym Chem 1980;18:2597–608.
[34] Lim WW, Mizumachi H. Fracture toughness of adhesive joints. II. Temperature and rate dependencies of mode I fracture toughness and adhesive tensile strength. J Appl Polym Sci 1995;57:55–61.
[35] Lim WW, Mizumachi H. Fracture toughness of adhesive joints. III. Temperature and rate dependencies of mode II fracture toughness and adhesive shear strength. J Appl Polym Sci 1997;63:835–41.
[36] Derail C, Allal A, Marin G, Tordjeman Ph. Relationship between viscoelastic and peeling properties of model adhesives. Part 1. Cohesive fracture. J Adhes 1997;61:123–57.
[37] Derail C, Allal A, Marin G, Tordjeman Ph. Relationship between viscoelastic and peeling properties of model adhesives. Part 2. The interfacial fracture domains. J Adhes 1998;68:203–28.
[38] Guiu A, Shanahan MER. Adhesion between semi-crystalline polymers: grafted PE/EVOH copolymer. Int J Adhes Adhes 2002;22:415–20.
[39] North WPT, Taylor CE. Dynamic-stress concentration using photoelasticity and a laser light source. Exp Mech 1966;6:337–41.